

Exploring Critical Overdensity Thresholds in Inflationary Models of Primordial Black Holes Formation

Ioanna D. Stamou ¹

¹*Service de Physique Théorique, C.P. 225, Université Libre de Bruxelles,
Boulevard du Triomphe, B-1050 Brussels, Belgium*

Abstract

In this paper we study the production of Primordial Black Holes (PBHs) from inflation in order to explain the Dark Matter (DM) in the Universe. The evaluation of the fractional PBHs abundance to DM is sensitive to the value of the threshold δ_c and the exact value of δ_c is sensitive to the specific shape of the cosmological fluctuations. Different mechanisms producing PBHs lead to different thresholds and hence to different fractional abundances of PBHs. In this study, we examine various classes of inflationary models proposed in the existing literature to elucidate the formation of PBHs and we evaluate numerically the associated threshold values. Having evaluated the thresholds we compute the abundances of PBHs to DM using the Press-Schechter approach and the Peak Theory. Given the influence of different power spectra on the thresholds, we investigate whether these inflationary models can successfully account for a significant fraction of DM. Moreover, we provide suggested values for the critical threshold. By examining the interplay between inflationary models, threshold values, and PBH abundances, our study aims to shed light on the viability of PBHs as a candidate for DM and contributes to the ongoing discussion regarding the nature of DM in the Universe.

1 Introduction

Dark Matter (DM) is considered as one of the biggest problem in Cosmology. Recent observations, such as the detection of Gravitational Waves emitted by a binary black hole merger [1–5], have reignited interest in the possibility that Primordial Black Holes (PBHs) could constitute a significant fraction of DM. The idea of PBHs was proposed in the 1970s by Hawking and Carr [6, 7]. The renewed detection of Gravitational Waves has revitalized the exploration of the connection between DM and PBHs.

In particular, there are numerous theoretical studies on the formation of PBHs from inflationary models, such as Refs. [8–42]. According to these studies an enhancement in the power spectrum at small scales can lead to PBHs formation, which could explain a significant fraction of DM (or even the whole DM) in the Universe. Many of these models are based on single field inflation with a near inflection point in the scalar potential, such as those of Refs. [11–23]. The drawback of these models is that a lot of fine-tuning in the underlying parameters is required. Other models with two-field inflation have been proposed [8, 24–30]. For instance, hybrid models have been intensely studied in the literature [9, 10, 31, 32]. The formation of PBHs in the majority of these models takes place in the radiation dominated epoch. In our study we only consider this class of models.

The formation of PBHs occurs when a cosmological perturbation collapses to a black hole if its amplitude δ exceeds a certain threshold value δ_c . Early analytical estimates of δ_c were based on a simplified Jeans length approximation, which gives $\delta_c \sim w$, where w is the equation of state [43]. More recent studies have refined this value by incorporating the theory of General Relativity, obtaining $\delta_c \sim 0.4$ in the radiation dominated era [44]. However, this analytical computation provides only a lower bound because it does not account for non-linear effects. Full numerical relativistic simulations are required to fully capture these effects, which recent studies

have shown to be dependent on the initial curvature profile, with $0.4 \leq \delta_c \leq 2/3$ [45–52]. Significant progress has been made in understanding the mechanism of PBH formation through detailed spherically symmetric numerical simulations that incorporate a non-linear approach [53–63].

It was previously remarked that the threshold for PBHs formation depends on the specific mechanism of inflation and the properties of the collapsing object, such as its mass, size, and initial density profile [47, 53–55, 59, 64, 65]. In addition to that, the abundances of DM from PBHs are extremely sensitive to the threshold and the exact value of the peak. In other words, the shape of the power spectrum leads to a different threshold and hence to a different abundance of PBHs to DM [46]. In the aforementioned inflationary models an acceptable value of the threshold is used and the fact that the critical threshold is depended on the shape of the power spectrum was neglected. As the evaluation of the fractional abundance of PBHs is crucial depended on the threshold and this threshold depends on the power spectrum, we believe that it should be tested that these models can indeed explain a significant fraction of DM. Therefore, as the exact value of the threshold has an important role in the calculation, it can lead to either ruling out or not inflationary models for producing PBHs as DM.

In this study we evaluate numerically the threshold for some classes of inflationary models presented in the literature. Specifically, we study the thresholds for the case of two inflation model with a non-canonical kinetic term [8], the case of hybrid model [9, 10] and the case of a single field with an inflection point [18]. Having these values for the threshold we evaluate the abundance of PBHs to DM. Instead of having an acceptable value for the threshold, we evaluate numerically these thresholds for each case. The advantage of these three models is that they allow the calculation of the evaluation of the critical threshold for just one parameter. One parameter dependence is needed in order to avoid a complicated numerical evaluation of the threshold from a power spectrum of a given model. Other models provided in the literature with same shapes of the power spectrum may not lead to one-to-one comparison of the shape and the critical threshold, as many parameters can change the results. However, the results of the critical value can be applied to the other models with similar shape of power spectrum. In this study, we can conclude if these models can predict a significant fraction of DM and we can propose a value for the threshold for those models.

The layout of this paper is as follows: in Section 2 we present the basic aspects for the threshold δ_c . In Section 3 we show the evaluation of δ_c for a given power spectrum. In Section 4 we present the calculation of the abundances of PBHs. In Section 5 we present the application of the previous analysis to inflationary models and especially to two field models, hybrid models and models with an inflection point. Finally, we draw our conclusions in Section 6.

2 The threshold δ_c

In this section we introduce the threshold of PBHs. Generally, the threshold for PBHs is determined by the density fluctuations in the early Universe, which can collapse under their own gravity to form black holes if they exceed a certain threshold value.

The PBHs are formed from cosmological fluctuations after re-entering the horizon. Under the assumption of spherical symmetry, the spacetime metric on the superhorizon scales can be given as

$$ds^2 = -dt^2 + a^2(t) \left[\frac{dr^2}{1 - K(r)r^2} + r^2 d\Omega^2 \right] = -dt^2 + a(t)^2 \exp(2\zeta(\hat{r})) [d\hat{r}^2 + \hat{r}^2 d\Omega^2] \quad (1)$$

where $a(t)$ is the scale factor and K and $\zeta(r)$ are the conserved comoving curvature perturbations defined at the superhorizon scales. Combining these expressions we have:

$$K(r)r^2 = -\hat{r}\zeta'(\hat{r})(2 + \hat{r}\zeta'(\hat{r})). \quad (2)$$

and the coordinates r and \hat{r} are connected as follows:

$$r = \hat{r} \exp(\zeta(\hat{r}))$$

$$\frac{dr}{\sqrt{1 - K(r)r^2}} = \exp(\zeta(\hat{r})) d\hat{r}. \quad (3)$$

As shown in [47, 53–55, 59] the shape of cosmological perturbations is related to the K and $\zeta(r)$ and so they are related to the power spectrum P_R . In other words, different scalar power spectrum profiles can result in varying thresholds.

The energy density profile is defined from:

$$\frac{\delta\rho}{\rho_b} \equiv \frac{\rho(r,t) - \rho_b(t)}{\rho_b(t)} = f(w) \left(\frac{1}{aH} \right)^2 \left(K(r) + \frac{r}{3} K'(r) \right) \quad (4)$$

where H is the Hubble parameter, ρ_b is the mean background energy density and $f(w)$ is:

$$f(w) = 3(1+w)/(5+3w) \quad (5)$$

with w is the equation of state $w = p/\rho$.

The criterion to define the PBHs formation can be given at the peak of the compactification function, which is defined as follows:

$$C \equiv 2 \frac{\delta M}{R(r,t)} \quad (6)$$

where R is the areal radius and $\delta M = M(r,t) - M_b(r,t)$. M is the Misner-Sharp mass and $M_b(r,t) = 4\pi\rho_b R^3/3$. If we define the expansion parameter ε as follows

$$\varepsilon = \frac{1}{a(t)r_m H(t)} = \frac{1}{a(t)\hat{r}_m \exp(\zeta) H(t)} \quad (7)$$

one can express the compactification function C at the leading order $O(\varepsilon^3)$ of the gradient expansion of Misner-Sharp equations as follows [49, 55, 66, 67]:

$$C \simeq f(w) K(r) r^2 = f(w) (1 - [1 + \hat{r} \zeta'(\hat{r})]^2). \quad (8)$$

The expression of energy density profile is valid if $\varepsilon \ll 1$. Finally, the threshold δ_c is equivalent to the peak value of the compactification function, $\delta_c = C(\hat{r}_m)$. Fluctuations with amplitude δ_m bigger than the threshold, $\delta_m > \delta_c$, can collapse to form PBHs, otherwise fluctuations with $\delta_m < \delta_c$ cannot lead to PBHs formation.

Having the assumption of spherically symmetric perturbation we define the dimensionless shape parameter q [47, 48] as:

$$q = -\frac{C''(r_m) r_m^2}{4C(r_m)}. \quad (9)$$

and in terms of \hat{r} it takes the form:

$$q = -\frac{C''(\hat{r}_m) \hat{r}_m^2}{4C(\hat{r}_m) \left(1 - \frac{C(\hat{r}_m)}{f(w)} \right)}. \quad (10)$$

This parameter is characterised from the width of the peak of the compactification function. We remark here that different profiles with same parameter q have the approximated same threshold δ_c in the case of radiation epoch [48].

3 The estimation of the threshold

There is a number of works where an analytical expression for the threshold δ_c was studied [7, 45, 48]. In our study we use this of Ref. [48]. In this section, we summarize the evaluation of the threshold for a given scalar power spectrum P_R . As we remarked previously, the shape of the power spectrum leads to a different threshold. This analysis is presented in Refs. [45–49].

In general, the power spectrum is given by

$$P_R(k) = \frac{k^3}{2\pi^2} |\mathcal{R}|^2 \quad (11)$$

with \mathcal{R} the curvature perturbation and k is the comoving wavenumber. A concise analysis of the power spectrum evaluation will be presented later. In this section we follow the steps of Ref. [49] in order to obtain the threshold δ_c for a given power spectrum. An equivalent analysis is presented in Ref. [45].

In order to obtain the threshold, one should consider the two point correlation function as:

$$g(\hat{r}) = \frac{1}{\sigma_0^2} \int_{-\infty}^{\infty} \frac{dk}{k} \frac{\sin(k\hat{r})}{k\hat{r}} P_R(k). \quad (12)$$

with

$$\sigma_0^2 = \int_{-\infty}^{\infty} dk \frac{P_R(k)}{k}. \quad (13)$$

The Eq. (12) connects the scalar power spectrum P_R with the two point correlation function.

As a first step in the calculation of the δ_c , we should locate the maximum value of the compactification function \hat{r}_m . The value of \hat{r}_m can be obtained by the root of the following equation:

$$\zeta'(\hat{r}_m) + \hat{r}_m \zeta''(\hat{r}_m) = 0 \quad (14)$$

where μ is the amplitude of curvature fluctuation and it is given as follows:

$$\mu = \zeta(\hat{r})/g(\hat{r}) \quad (15)$$

or

$$\mu = \frac{\pm \sqrt{1 - C(\hat{r}_m)/f(w)} - 1}{g'(\hat{r}_m)\hat{r}_m}. \quad (16)$$

The critical amplitude, μ_c , is obtained at $C(r_m) = \delta_c$.

In order to obtain the threshold we define the function

$$G(\hat{r}_m) = \frac{g'(\hat{r}_m) - \hat{r}_m^2 g'''(\hat{r}_m)/2}{g'(\hat{r}_m)}. \quad (17)$$

The threshold δ_c can be given from the following expressions:

$$q = G(r_m) \frac{1}{\sqrt{1 - \delta_c(q)/f(w)}} \frac{1}{(1 + \sqrt{1 - \delta_c(q)/f(w)})} \quad (18)$$

where δ_c is given:

$$\delta_c = \frac{4}{15} e^{-1/q} \frac{q^{1-5/2q}}{\Gamma(\frac{5}{2q}) - \Gamma(\frac{5}{2q}, \frac{1}{q})}. \quad (19)$$

The dimensionless parameter q given in Eq. (18) is the shape parameter and it is defined as the shape around the peak of the compactification function given previously in Eq.(9). The Eq. (19) is an analytical expression to calculate the threshold δ_c as a function of the shape parameter q in radiation era [48]. Finally, Γ is the incomplete gamma function.

4 The PBHs production

Until now, we have introduced the evaluation of the thresholds δ_c . As we study the possibility of PBHs to explain the DM, we introduce the evaluation of the fraction of PBHs to DM, f_{PBH} . In this section we summarize the calculation of f_{PBH} .

The present abundance of PBHs is given by the integral:

$$f_{PBH} = \int d \ln M \frac{\Omega_{PBH}}{\Omega_{DM}} \quad (20)$$

and the fractional abundance of PBHs to DM is:

$$\frac{\Omega_{PBH}}{\Omega_{DM}} = \frac{\beta(M_{PBH}(k))}{8 \times 10^{-16}} \left(\frac{\gamma}{0.2} \right)^{3/2} \left(\frac{g(T_f)}{106.75} \right)^{-1/4} \left(\frac{M_{PBH}}{10^{-18} g} \right)^{-1/2}, \quad (21)$$

where β is the mass fraction of Universe to collapse to PBHs, γ is the correction factor which depends on the gravitational collapse, M_{PBH} is the mass of PBHs and $g(T_f)$ is the effective number of degrees of freedom when the PBHs are produced. The mass of PBHs, M_{PBH} , is associated with the mass inside the Hubble horizon as:

$$M_{PBH} = \gamma M_H = \gamma \frac{4}{3} \pi \rho H^{-3} \quad (22)$$

where ρ is the energy density of the Universe during the collapse. The M_{PBH} is given as

$$M_{PBH} = 10^{18} \left(\frac{\gamma}{0.2} \right) \left(\frac{g(T_f)}{106.75} \right)^{-1/6} \left(\frac{k}{7 \times 10^{13} \text{Mpc}^{-1}} \right)^{-2} g. \quad (23)$$

We choose $\gamma = 0.8$ and $g_* = 106.75$ [43].

The variance of curvature perturbation σ_δ is related to the power spectrum by the following expression:

$$\sigma_\delta^2(M_{PBH}(k)) = \frac{4(1+w)^2}{(5+3w)^2} \int \frac{dk'}{k'} \left(\frac{k'}{k} \right)^4 P_R(k') \tilde{W}^2 \left(\frac{k'}{k} \right) \quad (24)$$

and for the i -th spectral momentum the smoothed density is give as:

$$\sigma_i^2(M_{PBH}(k)) = \frac{4(1+w)^2}{(5+3w)^2} \int \frac{dk'}{k'} \left(\frac{k'}{k} \right)^4 (k')^{2i} P_R(k') \tilde{W}^2 \left(\frac{k'}{k} \right) \quad (25)$$

where the equation of state, w , in radiation dominated epoch is equal to $1/3$. $\tilde{W} \left(\frac{k'}{k} \right)$ is the Fourier transform of the window function. In the following we assume a Gaussian window function.

The fraction β can be evaluated with the Press Schecter approach (PS) [68] or with the Peak Theory (PT) [46, 69–71]. In PS approach the mass fraction, β_{PS} , is given by the probability that the overdensity δ is above a certain threshold of collapse, denoted as δ_c . To estimate the probability of PBHs formation and establish a connection between the collapse threshold and the power spectrum, we make the assumption that curvature perturbations can be described by Gaussian statistics. This assumption allows us to analyze the formation probability of PBHs and investigate how it relates to the characteristics of the power spectrum. The fraction β_{PS} for this approach reads as:

$$\beta_{PS}(M_{PBH}) = \frac{1}{\sqrt{2\pi\sigma_\delta^2(M)}} \int_{\delta_c}^{\infty} d\delta e^{\frac{-\delta^2}{2\sigma_\delta^2(M)}} = \frac{1}{2} \text{Erfc} \left(\frac{\delta_c}{\sqrt{2}\sigma_\delta} \right). \quad (26)$$

The Eq. (26) is computed using the incomplete gamma function:

$$\beta_{PS}(M_{PBH}) = \frac{\Gamma \left(\frac{1}{2}, \frac{\delta_c^2}{2\sigma_\delta^2} \right)}{2\sqrt{\pi}}. \quad (27)$$

The PS approach has been found to underestimate the fractional abundances of PBHs by approximately two orders of magnitude [18, 72]. For this reason we consider the PT as well. The peak number density is given by

$$n_{peak} = \int_{v_c}^{\infty} \mathcal{N}(v) dv = \frac{\sigma_2^3}{(2\pi)^2 (\sqrt{3}\sigma_1)^3} \int_{v_c}^{\infty} dv \tilde{G}(\kappa, v) e^{-v^2/2} \quad (28)$$

where $v \equiv \delta/\sigma_0$ and v_c corresponds to this value at the threshold δ_c . The function \tilde{G} is given from:

$$\tilde{G}(\kappa, v) = \int_0^{\infty} \frac{f(x)}{\sqrt{2\pi(1-\kappa^2)}} \exp \left[-\frac{(x - \kappa v)^2}{2(1-\kappa^2)} \right] dx \quad (29)$$

where

$$f = \frac{x^3 - 3x}{2} \left[\text{erf} \left(\sqrt{\frac{5}{2}} x \right) + \text{erf} \left(\sqrt{\frac{5}{8}} x \right) \right] + \sqrt{\frac{2}{5\pi}} \left[\left(\frac{31x^2}{4} + \frac{8}{5} \right) e^{-5x^2/8} + \left(\frac{x^2}{2} - \frac{8}{5} \right) e^{-5x^2/2} \right]. \quad (30)$$

The mass fraction in PT is given from:

$$\beta_{PT} = \frac{1}{\sqrt{2\pi}} \left(\frac{\sigma_2}{(aH)(\sqrt{3}\sigma_1)} \right)^3 \int_{v_c}^{\infty} \tilde{G}(\kappa, v) \exp\left[-\frac{v^2}{2}\right] dv. \quad (31)$$

A recent approximation gives good results in comparison with the exact numerical PT [72]. According to this approximation the β_{PT} function can be approximated by:

$$\beta_{appr} = \frac{1}{\sqrt{2\pi}} Q^3 (v_c^2 - 1) \exp\left[-\frac{v_c^2}{2}\right] \quad (32)$$

where $Q = \sigma_1/(aH\sqrt{3}\sigma_\delta)$. In the following we will use this approximation.

As we can notice in this section from the mass fraction β is sensitive to the exact value of the threshold. In both studies of PS and PT, Eqs.(27) and (31), the value of β and, hence, the value of the f_{PBH} is exponentially sensitive to the value of the threshold δ_c . A slightly different threshold can give different results and that is the reason for the numerical evaluation of the threshold.

5 Threshold in inflationary models

In this section we present the calculation of the threshold δ_c for different classes of models proposed in the literature, which are a two-field model with a non-canonical kinetic term, a hybrid model with a waterfall trajectory and a model with an inflection point in the effective scalar potential. Specifically, in the hybrid model the parameters can be combined to just one parameter, which will be introduced later, defined as Π , as it is suggested in [9]. Hence, with just one parameter we can derive the height and width of power spectrum. For the other two models the parameters which are needed for fixing the width and height of the power spectrum is $b_{1,2}$ [8, 18]. The other parameters fix the position of the power spectrum and they are important in order to have a good explanation of the abundances of PBHs to dark matter at the window of $[10^{-16} - 10^{-10}] M_\odot$ and simultaneously fitted with the observable constraints of inflation at CMB scales [18]. However, they do not affect the height and width. So, we examine if these models can predict a significant fraction of DM. We define the parameter of each mechanism, which is responsible for the height and width of power spectrum. Finally, we evaluate the threshold and we propose a value in order these models can explain the maximum of PBHs abundances.

5.1 Threshold in two field model with non-canonical kinetic term

In this section we evaluate the threshold and the abundance of PBHs to DM by the two-field model studied in Ref. [8]. This two-field model is characterized by two stages of inflation with a large non-canonical kinetic coupling, which connects the two fields [8, 24–28]. The perturbations at small scales are dramatically enhanced by the sharp feature in the form of non-minimal coupling.

In particular, the action of a two-field toy model is given by the expression:

$$S = \int d^4x \sqrt{-g} \left[\frac{M_P^2}{2} R - \frac{1}{2} (\partial\phi)^2 - e^{-b_1\phi} (\partial\chi)^2 + V(\phi, \chi) \right] \quad (33)$$

where M_P is the reduced Planck mass. The potential is given as follows:

$$V(\phi, \chi) = V_0 \frac{\phi^2}{\phi_0^2 + \phi^2} + \frac{m_\chi^2}{2} \chi^2 \quad (34)$$

where ϕ is a canonical scalar field, χ is a non-canonical scalar field and b_1 an interaction between the fields. V_0 , ϕ_0 and m_χ are parameters. In the following we consider the choices of parameters in [8]: $V_0/(m_\chi M_P)^2 = 500$ and $\phi_0 = \sqrt{6} M_P$.

As we mentioned before, for the computation of δ_c we need as a first step to evaluate the primordial power spectrum. The power spectrum is evaluated numerically by solving the perturbation of the fields. For this reason

we briefly refer to this evaluation. The equations below are written for n -fields, but one can easily obtain those for one or two fields. More details can be found in [73].

Generally, the equation of the fields ϕ^i using efold time is given from (we work in $M_P = 1$):

$$\ddot{\phi}^c + \Upsilon_{ab}^c \dot{\phi}^a \dot{\phi}^b + \left(3 - \frac{1}{2} \dot{\sigma}^2\right) \dot{\phi}^c + \left(3 - \frac{1}{2} \dot{\sigma}^2\right) \frac{V^c}{V} = 0 \quad (35)$$

where dots represent the derivative in respect to efold time and indices $i = a, b, c$ represent derivatives with respect to the field. Υ_{ab}^c denotes the Christofel symbol in respect to the fields:

$$\Upsilon_{ab}^c = \frac{1}{2} G^{cd} (G_{da,b} + G_{db,a} - G_{ab,d}), \quad (36)$$

where G_{ij} is the field metric. By $\dot{\sigma}$ we denote the velocity field which is given as follows:

$$\dot{\sigma}^2 = G_{ab} \dot{\phi}^a \dot{\phi}^b. \quad (37)$$

The Hubble parameter is given by:

$$H^2 = \frac{V}{3 - \frac{1}{2} \dot{\sigma}^2} \quad (38)$$

and the slow-roll parameter ϵ_1 is given from:

$$\epsilon_1 = \frac{1}{2} \dot{\sigma}^2. \quad (39)$$

The equation for the perturbations $\delta\phi^2$ of the fields are given by:

$$\begin{aligned} \delta\ddot{\phi}^c + (3 - \epsilon_1) \delta\dot{\phi}^c + 2\Upsilon_{ab}^c \dot{\phi}^a \delta\dot{\phi}^b + \left(\Upsilon_{ab,d}^c \dot{\phi}^a \dot{\phi}^b + \frac{V_d^c}{H^2} - G^{ca} G_{ab,d} \frac{V^b}{H^2}\right) \delta\phi^d \\ + \frac{k^2}{a^2 H^2} \delta\phi^c = 4\Psi\dot{\phi}^c - 2\Psi \frac{V^c}{H^2} \end{aligned} \quad (40)$$

and the equation for the Bardeen potential Ψ is given by:

$$\ddot{\Psi} + (7 - \epsilon_1) \dot{\Psi} + \left(2 \frac{V}{H^2} + \frac{k^2}{a^2 H^2}\right) \Psi = -\frac{V_c}{H^2} \delta\phi^c. \quad (41)$$

In this analysis we suppose that we are initially in Bunch-Davies vacuum. The power spectrum is given from the equation:

$$P_R = \frac{k^3}{(2\pi)^2} (R_i^2) \quad (42)$$

where

$$R_i = \Psi + H \sum_i^{N_{fields}} \frac{\dot{\phi}_i \delta\phi_i}{\dot{\phi}_i^2}. \quad (43)$$

In Fig. 1 (left panel) we show the power spectrum for different values of the parameter b_1 given in the kinetic term of the action (33). As one can notice the peak height and the width of the power spectrum depend on the parameter b_1 . For the given power spectra we evaluate the value of the threshold following the steps of the Section 3. The threshold, which is finally given from the Eq. (19), is depicted in the right panel of Fig. 1 as a function of b_1 (black line). Therefore one can notice that different profiles of power spectrum lead to different thresholds δ_c .

Finally, we evaluate the abundance of PBHs to DM using the PT formalism in Eq. (20). In the right panel of Fig. 1 we present the specific choice of the value of the b_1 in order to explain the whole amount of DM (orange dashed line). We observe that this model requires a threshold at around $\delta_c = 0.515$. It is also imperative to verify that the fractional abundance Ω_{PBH}/Ω_{DM} , given in Eq. (21), does not exceed 1. In the specific case we have investigated, the value slightly surpasses 1, leading to the need to explore smaller but notable abundances. Therefore, for obtaining the maximum DM we need a slighter smaller power spectrum and thus a slighter smaller threshold. To sum up, this inflationary mechanism with two fields and a large coupling, which connects these two fields, can explain a significant amount of DM from PBHs formation.

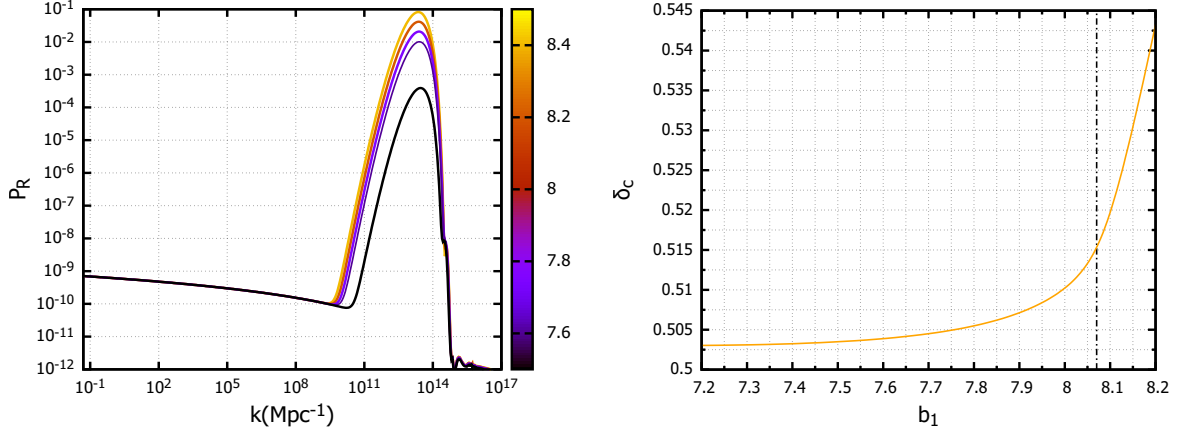


Figure 1: Left: Primordial power spectrum for different values of b . Right: The value of δ_c versus the value of the b_1 . The dashed line corresponds the choice of parameter b_1 in order to define all the dark matter in the Universe.

5.2 Threshold in hybrid model

Hybrid models for explaining the PBHs have already been proposed [9, 10]. According to these models, large curvature perturbations can be generated during a mild waterfall trajectory. In particular, these models are in the framework of two field inflation, where one field acquires tachyonic solution in the critical point and the other, which plays the role of the inflaton, becomes unstable. The analysis of the background dynamics is decomposed in two phases: a slow-roll phase until the critical point and a second waterfall phase till the end of the inflation. The calculation of the inflationary observables during these phases has been performed analytically in the slow-roll approximation [9, 74]. In this section we present the two field hybrid model [10] for explaining the DM and we evaluate the δ_c and then the abundances of PBHs to DM.

The F-term hybrid model in the globally supersymmetric renormalizable superpotential reads as follows [75–77]:

$$W = \kappa S(\Psi_1 \Psi_2 - \frac{M^2}{2}), \quad (44)$$

where Ψ_1, Ψ_2 are chiral superfields, the scalar component of the superfield, S is the gauge singlet inflaton field, κ is a dimensionless coupling constant and M is a mass. The scalar potential in hybrid models is given from

$$V_F^{\text{SUSY}} = \Lambda \left[\left(1 - \frac{\psi^2}{M^2} \right)^2 + \frac{2\phi^2\psi^2}{M^4} \right], \quad (45)$$

where we have assumed $\Lambda = \kappa^2 M^4 / 4$. In order to fix the non-canonical kinetic term we have $|S| = \phi / \sqrt{2}$ and $|\Psi_1| = |\Psi_2| = \psi / \sqrt{2}$. The potential is flat along the direction $\psi = 0$, $|\phi| > |\phi_c| = M$ and is given by a constant value for the energy density $V = \kappa^2 m^4$. The field ψ develops tachyonic solutions if

$$\kappa^2(-M^2 + \phi^2 + 6\psi^2) < 0. \quad (46)$$

Along the flat direction this condition becomes:

$$\phi_c^2 < M^2. \quad (47)$$

The value of the field ϕ_c denotes the critical point, as below this value the field develops tachyonic solutions. The inflaton ϕ field moves through the valley until it reaches the critical point. After that the other field, which is called waterfall, acquires tachyonic solution and the inflaton moves through the waterfall. Finally, the inflation ends in false vacuum. A potential which leads to enhancement of power spectrum and is derived from hybrid model is given as follows [9, 10]:

$$V_{\text{hybrid}} = \Lambda \left[\left(1 - \frac{\psi^2}{M^2} \right)^2 + \frac{2\phi^2\psi^2}{M^4} + a_1(\phi - \phi_c) + a_2(\phi - \phi_c)^2 \right] \quad (48)$$

where a_1 and a_2 are dimensionful parameters. These parameters play a crucial role in shaping the characteristics of the potential and directly influence the behavior of the system at the critical point

The power spectrum of this two-field potential can be analytically estimated by employing the slow-roll approximation and dividing the solution into two distinct phases [9, 74]. In the first phase, inflation is solely driven by the inflaton, while the influence of the other field is considered negligible. However, as the inflationary process progresses, the terms associated with the other field gradually begin to dominate, leading to a significant impact on the dynamics of the system and this signifies the onset of the second phase. The approximated power spectrum is given from the following expression [9]:

$$P_R = \frac{1}{4\pi^2} \frac{\Lambda}{3M_P^2} \left(\frac{1}{a_1^2 M_P^4} + \frac{M^4}{64M_P^4 \xi_2^2 \psi_k^2} \right) \approx \frac{1}{4\pi^2} \frac{\Lambda}{3M_P^2} \frac{M^4}{64M_P^4 \psi_k^2 \xi_2^2} \quad (49)$$

where

$$\xi_2 = -\frac{\sqrt{a_1} \chi_2 M}{2}, \quad \text{with} \quad \chi_2 = \ln \left(\frac{M^{3/2} \sqrt{a_1}}{2\psi_0} \right). \quad (50)$$

and

$$\psi_k = \psi_0 e^{\chi_k}, \quad \text{with} \quad \chi_k = \frac{4a_1 M_P^4}{M^3} \left(\frac{\chi_2^{1/2} M^{3/2}}{2M_P^2 \sqrt{a_1}} + \frac{M \phi_c^{1/2}}{4M_P^2 a_1^{1/2} x_2^{1/2}} - N \right)^2. \quad (51)$$

The approximation (49) is in good agreement with the numerical evaluation of the power spectrum, as it is shown in Refs. [9, 10]. For this reason we use this expression for the computation of the thresholds. Interestingly, it is possible to characterize any of the quantities in this expression by the combination Π :

$$\Pi = \frac{M \sqrt{\phi_c}}{M_P^2 \sqrt{a_1}}. \quad (52)$$

Hence in the next we use this parameter for the evaluation of the threshold.

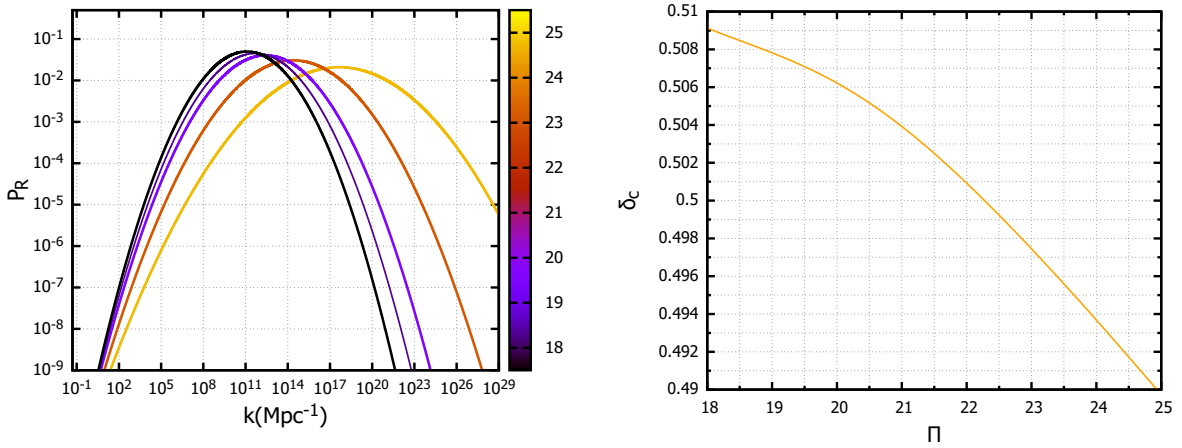


Figure 2: Hybrid model. Left: The power spectrum for different values of Π . Right: The value of δ_c versus the value of the Π .

In the left panel of Fig.2 we depict the power spectrum of Eq.(49) for different values of the parameter Π . We plot the spectra in respect to the comoving wavenumber k , which is connected to the number of e-folds as $k = k_* e^N$ and k_* is the pivot scale. In the right panel of Fig.2 we repeat the calculation for the threshold δ_c analyzed in Section 3. It is evident that larger values of the power spectrum width lead to a decrease in the corresponding threshold. This result aligns with the findings of Ref. [45], where the study focuses on the Gaussian and lognormal power spectra. As the width of the power spectrum increases, the shape parameter q decreases, indicating that the participation of multiple modes in the collapse results in a flatter compactification function [45].

Through this work we used PT instead of PS approach. To illustrate the contrast between these two methodologies we present a comparison in Fig.3 of how the f_{PBH} varies with respect to the parameter Π . In this figure

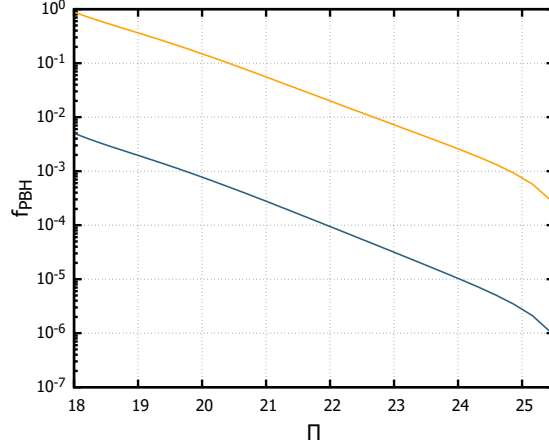


Figure 3: The fraction abundance of PBHs in the case of hybrid models.

we display the computed PBH abundance using both the PS (blue line) and PT (orange line) approaches. Remarkably, a significant disparity emerges between the PS approach and PT. When employing the PS approach, it is shown that we cannot explain a remarkable amount of DM. The fraction abundances increase as the value of Π decreases. However, in order to have such abundances we need the peak less than 10^{-8} and these regions are restricted from microlensing for Subaru (HSC), Eros/Macho/Ogle [78–80], ultra faint dwarf (UFD) [81] and CMB measurements [82].

In contradiction to PS approach, we observe a notable fraction of $\mathcal{O}(1)$ with the PT at the values of $\Pi = 18$. These findings highlight the effectiveness of the PT approach, as it offers the opportunity to potentially explain even the whole DM, thus yielding valuable insights for further exploration and analysis. Moreover, it is of utmost importance to ensure that the maximum value of the ratio $\Omega_{\text{PBH}}/\Omega_{\text{DM}}$ does not exceed 1. In this particular instance, we have determined that this value is lower than one, and so we can elucidate the whole DM content. Therefore, the hybrid models can obtain even the whole DM and the value of the threshold can be at around $\delta_c = 0.51$.

5.3 Threshold in model with an inflection point

An intriguing possibility in the framework of inflation is that the existence of an inflection point in the single field potential could provide an explanation for the generation of PBHs and subsequently account for a significant portion of the DM in the Universe. This mechanism arises when the slow-roll parameter, represented by ε_1 in Eq. (39), acquires a substantial value, resulting in the violation of the slow roll approximation. Importantly, this parameter remains below one, allowing inflation to continue. Following this, a phase emerges where the inflaton remains nearly constant, leading to a local amplification. During this plateau, the power spectrum experiences enhancement, facilitating the production of PBHs during the radiation-dominated phase of the early Universe. A lot of works have adopted the idea of an inflection point Refs. [8–21].

In many previous works, a value of δ_c in the range of acceptance has been used. Generally, one can find the exact value of δ_c for these models and then with fine tuning of the parameters which give the peak height, they can have a significant fraction of DM. For the study of single field inflation with an inflection point we present the model [18]. Similar result one can obtain for other models as well.

The model in Ref. [18] is embedded in no scale supergravity theory. The Kähler potential and superpotential are given from Eqs.:

$$\begin{aligned}
 K &= -3 \ln \left(1 - \frac{|y_1|^2}{3} - \frac{|y_2|^2}{3} \right), \\
 W &= m \left(-y_1 y_2 + \frac{y_2 y_1^2}{l\sqrt{3}} \right) \left(1 + c_2 e^{-b_2 y_1^2 y_1^2} \right)
 \end{aligned} \tag{53}$$

where y_1 and y_2 are chiral fields and l , b_2 and c_2 are parameters. The inflationary direction can be fixed assuming one field of these fields as the inflaton and the other as the modulo one. The analysis is presented in Refs [83,84].

The scalar potential V can be expressed in terms of the Kähler potential, K and the superpotential W :

$$V = e^{K/M_P^2} \left[(K^{-1})^i_{\bar{j}} \left(W^{\bar{j}} + \frac{W K^{\bar{j}}}{M_P^2} \right) \left(\bar{W}_i + \frac{\bar{W} K_i}{M_P^2} \right) - \frac{3|W|^2}{M_P^2} \right] \quad (54)$$

where $(K^{-1})^i_{\bar{j}}$ is the inverse of Kähler metric and $K^i = \partial K / \partial \Phi_i$. After the evaluation of the potential and concerning the non-canonical kinetic term of the Lagrangian, one can obtain an inflection point in the effective scalar potential. One should also take into account specific values for the parameters in order to obtain significant peaks at small scales in the effective scalar potential. In this analysis we adopt the parameters of Ref [18].

In Fig.4 (left panel) we depict the power spectrum as a function of the comoving wavenumber k for different choice of the parameter b . One can notice that a lot of fine tuning is required for obtaining a capable peak height of the power spectrum. For the evaluation of power spectrum we solve numerically the perturbation of the field, as they given from the differential equations (40) reduced in the single field case. Finally we derive the power spectrum from Eq. (42).

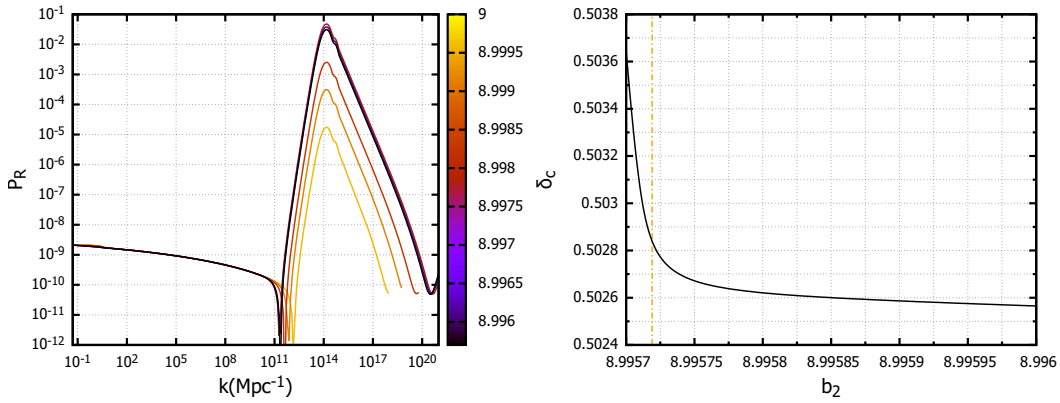


Figure 4: Left: The power spectrum for many choices of parameter b_2 . We choose $l = 1.0002$ and $c_2 = 14$. Right: The corresponding thresholds as a function of b_2 .

In the right panel of Fig.4 we depict the evaluated thresholds δ_c for some choices of the parameter b_2 with the formalism from Section 3. The dashed line in the right panel corresponds to the case where we have $f_{\text{PBH}} = 1$. The abundances of PBHs is calculate with the PT, as before. However, it is important to ensure that the maximum value of the ratio $\Omega_{\text{PBH}}/\Omega_{\text{DM}}$ does not exceed 1. The results are similar to the case of two field models with a large curvaton field. This value slightly surpasses 1, leading to the need to explore smaller abundances of PBHs. Therefore, inflationary models with an inflection point can predict a significant amount the DM from PBHs with the value of the threshold at around $\delta_c = 0.503$.

Nevertheless, the drawback of these models is that a lot of fine tuning to the interlining parameters is required. An additional problem for these models is that the one loop correction at large scales are too large to accept the validity of perturbation theory [85–88].

6 Conclusions

The formation of PBHs has been the subject of study for decades, with recent advances in numerical simulations providing a more complete understanding of the mechanism involved. The production of PBHs can be explained by a significant enhancement in the scalar power spectrum at small scales. In this work we study the production of PBHs from inflationary models by concerning the evaluation of the threshold δ_c .

Specifically, we study the evaluation of the threshold δ_c in some proposed mechanisms of producing PBHs in the framework of inflation. The first mechanism is based on a two field model with a non-canonical kinetic term, which is responsible for an important enhancement in the scalar power spectrum. The second one is based on a hybrid model characterized by a waterfall trajectory. The last mechanism is a single inflation with an inflection point in the effective scalar potential. These three models facilitate the computation of the critical

threshold by depending on only one parameter, as previously explained. A single parameter dependence is necessary to avoid complex numerical evaluation of thresholds from the power spectrum of a given model.

After evaluating the thresholds for PBHs formation, we calculate the fractional abundance of PBHs in relation to DM. Two approaches were used for this calculation: the PS approach and the PT. We observed that the PS approach tends to underestimate the results, thus necessitating the adoption of an approximation based on the PT. Our findings indicate that mechanisms based on both two-field inflation and single-field inflation with an inflection point have the ability to account for a significant fraction observed DM in the Universe, given specific parameter choices.

Furthermore, we have shown that the mechanism of a mild waterfall in the hybrid model has the capability to account for the entirety of the observed DM content in the Universe. Notably, when comparing the results obtained from the PS approach with those from the PT, it becomes evident that the PS approach yields lower values for the abundances in contrast to the PT approach. Consequently, while the PS approach imposes constraints on these models in order to explain only a fraction of the DM, the PT evaluation of the fraction provides the potential to explain even the entire DM. This discrepancy underscores the enhanced effectiveness and broader explanatory power of the PT approach in understanding the origins of DM in the Universe.

Finally, it is worth noting that in all the investigated models, the threshold value consistently converges around 0.51. This consistent threshold value holds significant implications for future comparative studies focused on the production of PBHs through inflationary processes. Understanding the precise threshold value provides a crucial benchmark for assessing the viability and efficiency of different inflationary scenarios in generating PBHs. These findings pave the way for more comprehensive and in-depth investigations into the underlying mechanisms that contribute to the formation of PBHs.

Acknowledgments

We would like to express our gratitude to S. Clesse, A. Escrivá, and I. Musco for their fruitful discussions and valuable insights. Their contributions have greatly enriched this work. I.D.S. acknowledges funding by the Belgian Fund for Research F.R.S.-FNRS through an Incentive Grant for Scientific Research (MIS).

References

- [1] B. P. Abbott, et al., Observation of Gravitational Waves from a Binary Black Hole Merger, *Phys. Rev. Lett.* 116 (6) (2016) 061102. [arXiv:1602.03837](#), doi:10.1103/PhysRevLett.116.061102.
- [2] B. P. Abbott, et al., GW170104: Observation of a 50-Solar-Mass Binary Black Hole Coalescence at Redshift 0.2, *Phys. Rev. Lett.* 118 (22) (2017) 221101, [Erratum: *Phys.Rev.Lett.* 121, 129901 (2018)]. [arXiv:1706.01812](#), doi:10.1103/PhysRevLett.118.221101.
- [3] B. P. Abbott, et al., GW170608: Observation of a 19-solar-mass Binary Black Hole Coalescence, *Astrophys. J. Lett.* 851 (2017) L35. [arXiv:1711.05578](#), doi:10.3847/2041-8213/aa9f0c.
- [4] B. P. Abbott, et al., GW170814: A Three-Detector Observation of Gravitational Waves from a Binary Black Hole Coalescence, *Phys. Rev. Lett.* 119 (14) (2017) 141101. [arXiv:1709.09660](#), doi:10.1103/PhysRevLett.119.141101.
- [5] B. P. Abbott, et al., GW151226: Observation of Gravitational Waves from a 22-Solar-Mass Binary Black Hole Coalescence, *Phys. Rev. Lett.* 116 (24) (2016) 241103. [arXiv:1606.04855](#), doi:10.1103/PhysRevLett.116.241103.
- [6] S. Hawking, Gravitationally collapsed objects of very low mass, *Mon. Not. Roy. Astron. Soc.* 152 (1971) 75.
- [7] B. J. Carr, S. W. Hawking, Black Holes in the Early Universe, *Monthly Notices of the Royal Astronomical Society* 168 (2) (1974) 399–415. [arXiv:https://academic.oup.com/mnras/article-pdf/168/2/399/8079885/mnras168-0399.pdf](#), doi:10.1093/mnras/168.2.399. URL <https://doi.org/10.1093/mnras/168.2.399>

- [8] M. Braglia, D. K. Hazra, F. Finelli, G. F. Smoot, L. Sriramkumar, A. A. Starobinsky, Generating PBHs and small-scale GWs in two-field models of inflation, JCAP 08 (2020) 001. arXiv:2005.02895, doi:10.1088/1475-7516/2020/08/001.
- [9] S. Clesse, J. García-Bellido, Massive primordial black holes from hybrid inflation as dark matter and the seeds of galaxies, Physical Review D 92 (2) (jul 2015). doi:10.1103/PhysRevD.92.023524.
- [10] V. C. Spanos, I. D. Stamou, Gravitational waves and primordial black holes from supersymmetric hybrid inflation, Phys. Rev. D 104 (12) (2021) 123537. arXiv:2108.05671, doi:10.1103/PhysRevD.104.123537.
- [11] G. Ballesteros, M. Taoso, Primordial black hole dark matter from single field inflation, Phys. Rev. D 97 (2) (2018) 023501. arXiv:1709.05565, doi:10.1103/PhysRevD.97.023501.
- [12] T.-J. Gao, Z.-K. Guo, Primordial Black Hole Production in Inflationary Models of Supergravity with a Single Chiral Superfield, Phys. Rev. D 98 (6) (2018) 063526. arXiv:1806.09320, doi:10.1103/PhysRevD.98.063526.
- [13] M. Cicoli, V. A. Diaz, F. G. Pedro, Primordial Black Holes from String Inflation, JCAP 06 (2018) 034. arXiv:1803.02837, doi:10.1088/1475-7516/2018/06/034.
- [14] I. Dalianis, A. Kehagias, G. Tringas, Primordial black holes from α -attractors, JCAP 01 (2019) 037. arXiv:1805.09483, doi:10.1088/1475-7516/2019/01/037.
- [15] J. Garcia-Bellido, E. Ruiz Morales, Primordial black holes from single field models of inflation, Phys. Dark Univ. 18 (2017) 47–54. arXiv:1702.03901, doi:10.1016/j.dark.2017.09.007.
- [16] J. M. Ezquiaga, J. Garcia-Bellido, E. Ruiz Morales, Primordial Black Hole production in Critical Higgs Inflation, Phys. Lett. B 776 (2018) 345–349. arXiv:1705.04861, doi:10.1016/j.physletb.2017.11.039.
- [17] D. V. Nanopoulos, V. C. Spanos, I. D. Stamou, Primordial Black Holes from No-Scale Supergravity, Phys. Rev. D 102 (8) (2020) 083536. arXiv:2008.01457, doi:10.1103/PhysRevD.102.083536.
- [18] I. D. Stamou, Mechanisms of producing primordial black holes by breaking the $SU(2,1)/SU(2) \times U(1)$ symmetry, Phys. Rev. D 103 (8) (2021) 083512. arXiv:2104.08654, doi:10.1103/PhysRevD.103.083512.
- [19] M. P. Hertzberg, M. Yamada, Primordial Black Holes from Polynomial Potentials in Single Field Inflation, Phys. Rev. D 97 (8) (2018) 083509. arXiv:1712.09750, doi:10.1103/PhysRevD.97.083509.
- [20] G. Ballesteros, J. Rey, F. Rompineve, Detuning primordial black hole dark matter with early matter domination and axion monodromy, JCAP 06 (2020) 014. arXiv:1912.01638, doi:10.1088/1475-7516/2020/06/014.
- [21] R. Mahbub, Primordial black hole formation in inflationary α -attractor models, Phys. Rev. D 101 (2) (2020) 023533. arXiv:1910.10602, doi:10.1103/PhysRevD.101.023533.
- [22] Y. Aldabergenov, A. Addazi, S. V. Ketov, Primordial black holes from modified supergravity, Eur. Phys. J. C 80 (10) (2020) 917. arXiv:2006.16641, doi:10.1140/epjc/s10052-020-08506-6.
- [23] I. D. Stamou, Primordial Black Holes And Gravitational Waves Based On No-Scale Supergravity, J. Phys. Conf. Ser. 2105 (8) (2021) 012008. arXiv:2111.14190, doi:10.1088/1742-6596/2105/1/012008.
- [24] D.-S. Meng, C. Yuan, Q.-G. Huang, Primordial black holes generated by the non-minimal spectator field (12 2022). arXiv:2212.03577.
- [25] M. Braglia, D. K. Hazra, L. Sriramkumar, F. Finelli, Generating primordial features at large scales in two field models of inflation, JCAP 08 (2020) 025. arXiv:2004.00672, doi:10.1088/1475-7516/2020/08/025.

- [26] S. R. Geller, W. Qin, E. McDonough, D. I. Kaiser, Primordial black holes from multifield inflation with nonminimal couplings, *Phys. Rev. D* 106 (6) (2022) 063535. [arXiv:2205.04471](#), [doi:10.1103/PhysRevD.106.063535](#).
- [27] M. Braglia, X. Chen, D. K. Hazra, Probing Primordial Features with the Stochastic Gravitational Wave Background, *JCAP* 03 (2021) 005. [arXiv:2012.05821](#), [doi:10.1088/1475-7516/2021/03/005](#).
- [28] R. Kallosh, A. Linde, Dilaton-axion inflation with PBHs and GWs, *JCAP* 08 (08) (2022) 037. [arXiv:2203.10437](#), [doi:10.1088/1475-7516/2022/08/037](#).
- [29] N. E. Mavromatos, V. C. Spanos, I. D. Stamou, Primordial black holes and gravitational waves in multi-axion-Chern-Simons inflation, *Phys. Rev. D* 106 (6) (2022) 063532. [arXiv:2206.07963](#), [doi:10.1103/PhysRevD.106.063532](#).
- [30] K. Boutivas, I. Dalianis, G. P. Kodaxis, N. Tetradis, The effect of multiple features on the power spectrum in two-field inflation, *JCAP* 08 (08) (2022) 021. [arXiv:2203.15605](#), [doi:10.1088/1475-7516/2022/08/021](#).
- [31] M. Braglia, A. Linde, R. Kallosh, F. Finelli, Hybrid α -attractors, primordial black holes and gravitational wave backgrounds (11 2022). [arXiv:2211.14262](#).
- [32] Y. Tada, M. Yamada, On the primordial black hole formation in hybrid inflation (4 2023). [arXiv:2304.01249](#).
- [33] A. Ashoorioon, A. Rostami, J. T. Firouzjaee, EFT compatible PBHs: effective spawning of the seeds for primordial black holes during inflation, *JHEP* 07 (2021) 087. [arXiv:1912.13326](#), [doi:10.1007/JHEP07\(2021\)087](#).
- [34] A. Ashoorioon, A. Rostami, J. T. Firouzjaee, Examining the end of inflation with primordial black holes mass distribution and gravitational waves, *Phys. Rev. D* 103 (2021) 123512. [arXiv:2012.02817](#), [doi:10.1103/PhysRevD.103.123512](#).
- [35] A. Ashoorioon, K. Rezazadeh, A. Rostami, NANOGrav signal from the end of inflation and the LIGO mass and heavier primordial black holes, *Phys. Lett. B* 835 (2022) 137542. [arXiv:2202.01131](#), [doi:10.1016/j.physletb.2022.137542](#).
- [36] K. M. Belotsky, V. I. Dokuchaev, Y. N. Eroshenko, E. A. Esipova, M. Y. Khlopov, L. A. Khromykh, A. A. Kirillov, V. V. Nikulin, S. G. Rubin, I. V. Svadkovsky, Clusters of primordial black holes, *Eur. Phys. J. C* 79 (3) (2019) 246. [arXiv:1807.06590](#), [doi:10.1140/epjc/s10052-019-6741-4](#).
- [37] M. Y. Khlopov, Primordial Black Holes, *Res. Astron. Astrophys.* 10 (2010) 495–528. [arXiv:0801.0116](#), [doi:10.1088/1674-4527/10/6/001](#).
- [38] V. C. Spanos, I. D. Stamou, Gravitational waves from no-scale supergravity, *Eur. Phys. J. C* 83 (1) (2023) 4. [arXiv:2205.05595](#), [doi:10.1140/epjc/s10052-022-11142-x](#).
- [39] S. Kawai, J. Kim, Primordial black holes and gravitational waves from nonminimally coupled supergravity inflation, *Phys. Rev. D* 107 (4) (2023) 043523. [arXiv:2209.15343](#), [doi:10.1103/PhysRevD.107.043523](#).
- [40] S. Kawai, J. Kim, Primordial black holes from Gauss-Bonnet-corrected single field inflation, *Phys. Rev. D* 104 (8) (2021) 083545. [arXiv:2108.01340](#), [doi:10.1103/PhysRevD.104.083545](#).
- [41] G. Ferrante, G. Franciolini, A. Iovino, Junior., A. Urbano, Primordial non-Gaussianity up to all orders: Theoretical aspects and implications for primordial black hole models, *Phys. Rev. D* 107 (4) (2023) 043520. [arXiv:2211.01728](#), [doi:10.1103/PhysRevD.107.043520](#).
- [42] A. Poisson, I. Timiryasov, S. Zell, Critical Points in Palatini Higgs Inflation with Small Non-Minimal Coupling (6 2023). [arXiv:2306.03893](#).

- [43] B. J. Carr, The primordial black hole mass spectrum.
- [44] T. Harada, C.-M. Yoo, K. Kohri, Threshold of primordial black hole formation, *Phys. Rev. D* 88 (8) (2013) 084051, [Erratum: *Phys.Rev.D* 89, 029903 (2014)]. [arXiv:1309.4201](#), [doi:10.1103/PhysRevD.88.084051](#).
- [45] I. Musco, V. De Luca, G. Franciolini, A. Riotto, Threshold for primordial black holes. II. A simple analytic prescription, *Phys. Rev. D* 103 (6) (2021) 063538. [arXiv:2011.03014](#), [doi:10.1103/PhysRevD.103.063538](#).
- [46] C. Germani, I. Musco, Abundance of Primordial Black Holes Depends on the Shape of the Inflationary Power Spectrum, *Phys. Rev. Lett.* 122 (14) (2019) 141302. [arXiv:1805.04087](#), [doi:10.1103/PhysRevLett.122.141302](#).
- [47] I. Musco, Threshold for primordial black holes: Dependence on the shape of the cosmological perturbations, *Phys. Rev. D* 100 (12) (2019) 123524. [arXiv:1809.02127](#), [doi:10.1103/PhysRevD.100.123524](#).
- [48] A. Escrivà, C. Germani, R. K. Sheth, Universal threshold for primordial black hole formation, *Phys. Rev. D* 101 (4) (2020) 044022. [arXiv:1907.13311](#), [doi:10.1103/PhysRevD.101.044022](#).
- [49] A. Escrivà, F. Kuhnel, Y. Tada, Primordial Black Holes (11 2022). [arXiv:2211.05767](#).
- [50] I. Musco, T. Papanikolaou, Primordial black hole formation for an anisotropic perfect fluid: Initial conditions and estimation of the threshold, *Phys. Rev. D* 106 (8) (2022) 083017. [arXiv:2110.05982](#), [doi:10.1103/PhysRevD.106.083017](#).
- [51] C.-M. Yoo, T. Harada, H. Okawa, Threshold of Primordial Black Hole Formation in Nonspherical Collapse, *Phys. Rev. D* 102 (4) (2020) 043526, [Erratum: *Phys.Rev.D* 107, 049901 (2023)]. [arXiv:2004.01042](#), [doi:10.1103/PhysRevD.102.043526](#).
- [52] A. Kehagias, I. Musco, A. Riotto, Non-Gaussian Formation of Primordial Black Holes: Effects on the Threshold, *JCAP* 12 (2019) 029. [arXiv:1906.07135](#), [doi:10.1088/1475-7516/2019/12/029](#).
- [53] M. Shibata, M. Sasaki, Black hole formation in the Friedmann universe: Formulation and computation in numerical relativity, *Phys. Rev. D* 60 (1999) 084002. [arXiv:gr-qc/9905064](#), [doi:10.1103/PhysRevD.60.084002](#).
- [54] A. Escrivà, C. Germani, R. K. Sheth, Analytical thresholds for black hole formation in general cosmological backgrounds, *JCAP* 01 (2021) 030. [arXiv:2007.05564](#), [doi:10.1088/1475-7516/2021/01/030](#).
- [55] T. Harada, C.-M. Yoo, T. Nakama, Y. Koga, Cosmological long-wavelength solutions and primordial black hole formation, *Phys. Rev. D* 91 (8) (2015) 084057. [arXiv:1503.03934](#), [doi:10.1103/PhysRevD.91.084057](#).
- [56] A. Escrivà, Simulation of primordial black hole formation using pseudo-spectral methods, *Phys. Dark Univ.* 27 (2020) 100466. [arXiv:1907.13065](#), [doi:10.1016/j.dark.2020.100466](#).
- [57] I. Musco, J. C. Miller, Primordial black hole formation in the early universe: critical behaviour and self-similarity, *Class. Quant. Grav.* 30 (2013) 145009. [arXiv:1201.2379](#), [doi:10.1088/0264-9381/30/14/145009](#).
- [58] I. Musco, J. C. Miller, A. G. Polnarev, Primordial black hole formation in the radiative era: Investigation of the critical nature of the collapse, *Class. Quant. Grav.* 26 (2009) 235001. [arXiv:0811.1452](#), [doi:10.1088/0264-9381/26/23/235001](#).
- [59] I. Musco, J. C. Miller, L. Rezzolla, Computations of primordial black hole formation, *Class. Quant. Grav.* 22 (2005) 1405–1424. [arXiv:gr-qc/0412063](#), [doi:10.1088/0264-9381/22/7/013](#).

- [60] I. Hawke, J. M. Stewart, The dynamics of primordial black-hole formation, *Classical and Quantum Gravity* 19 (14) (2002) 3687. doi:10.1088/0264-9381/19/14/310.
- [61] J. C. Niemeyer, K. Jedamzik, Near-critical gravitational collapse and the initial mass function of primordial black holes, *Phys. Rev. Lett.* 80 (1998) 5481–5484. arXiv:astro-ph/9709072, doi:10.1103/PhysRevLett.80.5481.
- [62] J. Bloomfield, D. Bulhosa, S. Face, Formalism for Primordial Black Hole Formation in Spherical Symmetry (4 2015). arXiv:1504.02071.
- [63] A. Escrivà, PBH Formation from Spherically Symmetric Hydrodynamical Perturbations: A Review, *Universe* 8 (2) (2022) 66. arXiv:2111.12693, doi:10.3390/universe8020066.
- [64] B. J. Carr, K. Kohri, Y. Sendouda, J. Yokoyama, New cosmological constraints on primordial black holes, *Phys. Rev. D* 81 (2010) 104019. arXiv:0912.5297, doi:10.1103/PhysRevD.81.104019.
- [65] B. Carr, K. Kohri, Y. Sendouda, J. Yokoyama, Constraints on primordial black holes, *Rept. Prog. Phys.* 84 (11) (2021) 116902. arXiv:2002.12778, doi:10.1088/1361-6633/ac1e31.
- [66] A. G. Polnarev, I. Musco, Curvature profiles as initial conditions for primordial black hole formation, *Class. Quant. Grav.* 24 (2007) 1405–1432. arXiv:gr-qc/0605122, doi:10.1088/0264-9381/24/6/003.
- [67] A. G. Polnarev, T. Nakama, J. Yokoyama, Self-consistent initial conditions for primordial black hole formation, *JCAP* 09 (2012) 027. arXiv:1204.6601, doi:10.1088/1475-7516/2012/09/027.
- [68] W. H. Press, P. Schechter, Formation of galaxies and clusters of galaxies by self-similar gravitational condensation, *The Astrophysical Journal* 187 (1974) 425. doi:10.1086/152650.
- [69] J. M. Bardeen, J. Bond, N. Kaiser, A. Szalay, The Statistics of Peaks of Gaussian Random Fields, *Astrophys. J.* 304 (1986) 15–61. doi:10.1086/164143.
- [70] S. Young, C. T. Byrnes, M. Sasaki, Calculating the mass fraction of primordial black holes, *JCAP* 07 (2014) 045. arXiv:1405.7023, doi:10.1088/1475-7516/2014/07/045.
- [71] C.-M. Yoo, T. Harada, J. Garriga, K. Kohri, Primordial black hole abundance from random Gaussian curvature perturbations and a local density threshold, *PTEP* 2018 (12) (2018) 123E01. arXiv:1805.03946, doi:10.1093/ptep/pty120.
- [72] Q. Wang, Y.-C. Liu, B.-Y. Su, N. Li, Primordial black holes from the perturbations in the inflaton potential in peak theory, *Phys. Rev. D* 104 (8) (2021) 083546. arXiv:2111.10028, doi:10.1103/PhysRevD.104.083546.
- [73] C. Ringeval, The exact numerical treatment of inflationary models, *Lect. Notes Phys.* 738 (2008) 243–273. arXiv:astro-ph/0703486.
- [74] H. Kodama, K. Kohri, K. Nakayama, On the waterfall behavior in hybrid inflation, *Prog. Theor. Phys.* 126 (2011) 331–350. arXiv:1102.5612, doi:10.1143/PTP.126.331.
- [75] E. J. Copeland, A. R. Liddle, D. H. Lyth, E. D. Stewart, D. Wands, False vacuum inflation with Einstein gravity, *Phys. Rev. D* 49 (1994) 6410–6433. arXiv:astro-ph/9401011, doi:10.1103/PhysRevD.49.6410.
- [76] A. D. Linde, Hybrid inflation, *Phys. Rev. D* 49 (1994) 748–754. arXiv:astro-ph/9307002, doi:10.1103/PhysRevD.49.748.
- [77] G. R. Dvali, Q. Shafi, R. K. Schaefer, Large scale structure and supersymmetric inflation without fine tuning, *Phys. Rev. Lett.* 73 (1994) 1886–1889. arXiv:hep-ph/9406319, doi:10.1103/PhysRevLett.73.1886.

- [78] F. Capela, M. Pshirkov, P. Tinyakov, Constraints on primordial black holes as dark matter candidates from capture by neutron stars, *Physical Review D* 87 (12) (jun 2013). doi:10.1103/physrevd.87.123524.
- [79] H. Niikura, M. Takada, N. Yasuda, R. H. Lupton, T. Sumi, S. More, T. Kurita, S. Sugiyama, A. More, M. Oguri, M. Chiba, Microlensing constraints on primordial black holes with subaru/HSC andromeda observations, *Nature Astronomy* 3 (6) (2019) 524–534. doi:10.1038/s41550-019-0723-1.
- [80] L. Wyrzykowski, et al., The OGLE View of Microlensing towards the Magellanic Clouds. IV. OGLE-III SMC Data and Final Conclusions on MACHOs, *Mon. Not. Roy. Astron. Soc.* 416 (2011) 2949. arXiv:1106.2925, doi:10.1111/j.1365-2966.2011.19243.x.
- [81] P. T. et. al., Limits on the macho content of the galactic halo from the EROS-2 survey of the magellanic clouds, *Astronomy & Astrophysics* 469 (2) (2007) 387–404. doi:10.1051/0004-6361:20066017.
- [82] Y. Ali-Haïmoud, M. Kamionkowski, Cosmic microwave background limits on accreting primordial black holes, *Physical Review D* 95 (4) (feb 2017). doi:10.1103/physrevd.95.043534.
- [83] J. Ellis, D. V. Nanopoulos, K. A. Olive, Starobinsky-like Inflationary Models as Avatars of No-Scale Supergravity, *JCAP* 10 (2013) 009. arXiv:1307.3537, doi:10.1088/1475-7516/2013/10/009.
- [84] J. Ellis, D. V. Nanopoulos, K. A. Olive, S. Verner, A general classification of Starobinsky-like inflationary avatars of $SU(2,1)/SU(2) \times U(1)$ no-scale supergravity, *JHEP* 03 (2019) 099. arXiv:1812.02192, doi:10.1007/JHEP03(2019)099.
- [85] J. Kristiano, J. Yokoyama, Ruling Out Primordial Black Hole Formation From Single-Field Inflation (11 2022). arXiv:2211.03395.
- [86] S. Choudhury, M. R. Gangopadhyay, M. Sami, No-go for the formation of heavy mass Primordial Black Holes in Single Field Inflation (1 2023). arXiv:2301.10000.
- [87] S. Choudhury, S. Panda, M. Sami, Galileon inflation evades the no-go for PBH formation in the single-field framework (4 2023). arXiv:2304.04065.
- [88] J. Fumagalli, Absence of one-loop effects on large scales from small scales in non-slow-roll dynamics (5 2023). arXiv:2305.19263.